B-physics computations from $N_f = 2$ tmQCD

N. Carrasco[(a)], **M. Ciuchini**[(b)], **P. Dimopoulos**[*(c,d)], **R. Frezzotti**[(d)], **V. Giménez**[(a)] **G. Herdoiza**[(f)], **V. Lubicz**[(g,b)], **C. Michael**[(h)], **E. Picca**[(g)], **G.C. Rossi**[(d)], **F. Sanfilippo**[(i)], **A. Shindler**[(j)], **L. Silvestrini**[(k)], **S. Simula**[(b)], **C. Tarantino**[(g,b)]

[(a)] *Departament de Física Teòrica and IFIC, Univ. de València-CSIC Dr. Moliner 50, E-46100 València, Spain, E-mail:* nuria.carrasco@uv.es, vicente.gimenez@uv.es

[(b)] *INFN, Sezione di Roma Tre,c/o Dipartimento di Fisica, Università Roma Tre, Via della Vasca Navale 84, I-00146 Rome, Italy, E-mail:* {ciuchini, simula}@roma3.infn.it

[(c)] *Centro Fermi - Museo Storico della Fisica e Centro Studi e Ricerche Enrico Fermi, Compendio del Viminale, Piazza del Viminale 1, I-00184 Rome, Italy,*

[(d)] *Dipartimento di Fisica, Università di Roma "Tor Vergata" and INFN Sezione "Tor Vergata", Via della Ricerca Scientifica 1, I-00133 Rome, Italy,*

E-mail: {dimopoulos,frezzotti,rossig}@roma2.infn.it

[(f)] *PRISMA Cluster of Excellence, Institut für Kernphysik,Johannes Gutenberg-Universität, D-55099 Mainz, Germany, E-mail:* herdoiza@kph.uni-mainz.de

[(g)] *Dipartimento di Fisica, Università Roma Tre, Via della Vasca Navale 84, I-00146 Rome, Italy, E-mail:* e.picca88@gmail.com, {lubicz, tarantino}@fis.uniroma3.it,

[(h)] *Theoretical Physics Division, Department of Mathematical Sciences, The University of Liverpool, Liverpool L69 3BX, UK, E-mail:* C.Michael@liverpool.ac.uk

[(i)] *Laboratoire de Physique Théorique (Bât. 210), Université Paris Sud, F-91405 Orasay-Cedex, France, E-mail:* francesco.sanfilippo@th.u-psud.fr

[(j)] *CERN, Physics Department, 1211 Geneva 23, Switzerland*

[(k)] *INFN, Sezione di Roma, c/o Dipartimento di Fisica, Sapienza, Università di Roma, Piazzale A. Moro, I-00185 Rome, Italy, E-mail:* Luca.Silvestrini@roma1.infn.it

We present an accurate lattice QCD computation of the b-quark mass, the B and B_s decay constants, the B-mixing bag-parameters for the full four-fermion operator basis, as well as estimates for ξ and $f_{Bq}\sqrt{B_q}$ extrapolated to the continuum limit and the physical pion mass. We have used $N_f = 2$ dynamical quark gauge configurations at four values of the lattice spacing generated by ETMC. Extrapolation in the heavy quark mass from the charm to the bottom quark region has been carried out using ratios of physical quantities computed at nearby quark masses, having an exactly known infinite mass limit.

31st International Symposium on Lattice Field Theory - LATTICE 2013
July 29 - August 3, 2013
Mainz, Germany

---

[*]Speaker.

1. Introduction

Many precision tests of the Standard Model (SM) and some proposals regarding stringent constraints on New Physics (NP) generalisations of the SM involve accurate studies of processes in the *b*-quark region. Experimental measurements on the leptonic decays $B \to \tau \nu_\tau$ and $B^0_{(s)} \to \mu^+ \mu^-$ need precise input information of the pseudoscalar decay constants f_B and f_{Bs} from lattice computations. Neutral *B*-meson oscillations are described, in the SM, by a single four-fermion operator whose matrix element (bag parameter) can be determined in lattice simulations. *B*-meson mixing, besides its crucial role in the Unitarity Triangle (UT) analysis, can provide important clues for detecting NP effects. The knowlegde of the values of the bag parameters of the complete four-fermion operator basis is required to obtain predictions about the NP scale for physics beyond the SM.

In these proceedings we report on computations of a number of *B*-physics hadronic observables performed within the European Twisted Mass Collaboration (ETMC). We have computed in the continuum limit, by making use of data at four values of the lattice spacing, the value of the *b*-quark mass, the pseudoscalar meson decay constants, f_B and f_{Bs} as well as their ratio. Moreover we have determined the bag parameters corresponding to the full four-fermion operator basis, as well as other interesting phenomenological quantities like ξ and $f_{Bq}\sqrt{B_i^{(q)}}$ ($i = 1, \ldots, 5$ and $q = d/s$). For a more detailed discussion of methods and results of this study the reader is referred to a recent ETMC publication [1] as well as to [2, 3]. First ETMC results of the *b*-quark mass using $N_f = 2 + 1 + 1$ gauge ensembles can be found in [4].

2. Lattice setup and computational details

We have employed $N_f = 2$ dynamical quark gauge configurations generated by ETMC ([5] – [7]) using Wilson twisted mass action tuned to maximal twist [8] at four values of the inverse bare gauge coupling, β. The lattice spacing values lie in the interval [0.05, 0.1] fm. Light quark mass values of the degenerate u/d quark produce light pseudoscalar mesons ("pions") in the range $280 \leq m_{PS} \leq 500$ MeV. We recall that the maximally twisted fermionic action offers the advantage of automatic $O(a)$ improvement for all the physical observables computed on the lattice [8]. Strange and charm quarks are treated in the quenched approximation. We have computed 2- and 3-point correlation functions using valence quark masses whose range is extended from the light sea quark mass up to 2.5-3 times the charm quark mass. The values of the light valence quark mass are set equal to the light sea ones. Renormalised quark masses are determined from the bare ones using the renormalisation constant (RC) $Z_\mu = Z_P^{-1}$, $\mu^R = \mu^{bare}/Z_P$. The Z_P values have been computed using RI/MOM techniques in [9]. Details of the ETMC determinations of light, strange and charm quark mass using $N_f = 2$ gauge ensembles are given in [10].

We have employed smeared interpolating operators in combination with APE smeared gauge links to compute 2- and 3- point correlation functions. With respect to the local fields the use of smeared ones reduce the overlap with the excited states and increased the projection onto the lowest energy eigenstate. We are able thus to extract heavy-light meson masses and matrix elements at relatively small Euclidean time separations. Moreover, as it is shown in [1], even better projection onto the ground state is achieved by employing a linear combination of smeared and lo-

cal interpolating fields. The optimal linear combination is determined by tuning the superposition parameter.

3. Computation of the b-quark mass and decay constants f_B and f_{Bs}

For the determination of B-physics observables for which the asymptotic behaviour is known from HQET, it is in general possible to use the ratio method described in ([1] – [3]). We briefly recall the computation for the b-quark mass. HQET suggests that in the static limit the heavy-light pseudoscalar meson mass obeys

$$\lim_{\mu_h^{\text{pole}} \to \infty} \left(M_{h\ell} / \mu_h^{\text{pole}} \right) = \text{const.} \tag{3.1}$$

We consider a set of heavy quark masses $(\overline{\mu}_h^{(1)}, \overline{\mu}_h^{(2)}, \cdots, \overline{\mu}_h^{(N)})$ having a fixed ratio, λ, between any two successive values: $\overline{\mu}_h^{(n)} = \lambda \overline{\mu}_h^{(n-1)}$. Throughout this work the "overline" notation for the quark masses denotes that they are renormalised in the $\overline{\text{MS}}$ scheme at 3 GeV. We construct properly normalised ratios namely, $y(\overline{\mu}_h^{(n)}, \lambda; \overline{\mu}_\ell, a)$, of the quantity in the lhs of Eq. (3.1) at nearby values of the heavy quark mass. Taking the static and continuum limit one gets the exact equation

$$\lim_{\overline{\mu}_h \to \infty} \lim_{a \to 0} y(\overline{\mu}_h^{(n)}, \lambda; \overline{\mu}_\ell, a) = 1 . \tag{3.2}$$

At each value of $\overline{\mu}_h^{(n)}$ we perform a combined chiral and continuum fit on the ratios to extract the quantity $y(\overline{\mu}_h) \equiv y(\overline{\mu}_h, \lambda; \overline{\mu}_{u/d}, a = 0)$. Discretisation effects in ratios are well under control. In Fig. 1(a) we show the data and the fit for the ratio that corresponds to the largest simulated pair of the heavy quark mass values. We describe the dependence of the ratio $y(\overline{\mu}_h)$ on $\overline{\mu}_h$ using the fit ansatz

$$y(\overline{\mu}_h) = 1 + \frac{\eta_1}{\overline{\mu}_h} + \frac{\eta_2}{\overline{\mu}_h^2}, \tag{3.3}$$

in which the constraint $\lim_{\overline{\mu}_h \to \infty} y(\overline{\mu}_h) = 1$ is implemented. The fit parameters could be, in general, functions of $\log(\overline{\mu}_h)$. However in the range of the currently explored heavy quark mass values this logarithmic dependence can be safely neglected. Data and fit are shown in Fig. 1(b). The final step consists in determining the b-quark mass value from the *chain* equation

$$y(\overline{\mu}_h^{(2)}) y(\overline{\mu}_h^{(3)}) \ldots y(\overline{\mu}_h^{(K+1)}) = \lambda^{-K} \frac{M_{hu/d}(\overline{\mu}_h^{(K+1)})}{M_{hu/d}(\overline{\mu}_h^{(1)})} \cdot \left[\frac{\rho(\overline{\mu}_h^{(1)}, \mu)}{\rho(\overline{\mu}_h^{(K+1)}, \mu)} \right], \tag{3.4}$$

where the function $\rho(\overline{\mu}_h^{(n)}, \mu)$, that is known up to N^3LO in perturbation theory, relates the $\overline{\text{MS}}$ renormalised quark mass (at the scale of $\mu = 3$ GeV) to the pole mass: $\mu_h^{\text{pole}} = \rho(\overline{\mu}_h, \mu) \overline{\mu}_h(\mu)$. In Eq. (3.4) λ, K and $\overline{\mu}_h^{(1)}$ have been chosen in such a way that $M_{hu/d}(\overline{\mu}_h^{(K+1)})$ coincides with the experimental value of the B-meson mass, $M_B = 5.279$ GeV. The quantity $M_{hu/d}(\overline{\mu}_h^{(1)})$ is the result of the combined chiral and continuum fit of pseudoscalar meson mass values evaluated at the reference heavy quark mass, $\mu_h^{(1)}$, that lies close to the charm quark mass. For $(\overline{\mu}_h^{(1)}, \lambda) = (1.05$ GeV, $1.1784)$, Eq. (3.4) is satisfied for $K = K_b = 9$. The b-quark mass in the $\overline{\text{MS}}$ scheme at 3 GeV is

$$m_b(m_b, \overline{\text{MS}}) = 4.29(9)(8)[12] \text{ GeV}, \tag{3.5}$$

3

where the first two errors are statistical and systematic, respectively. Adding them in quadrature gives the total error in the square brackets. Having calculated the value of the *b*-quark mass, we
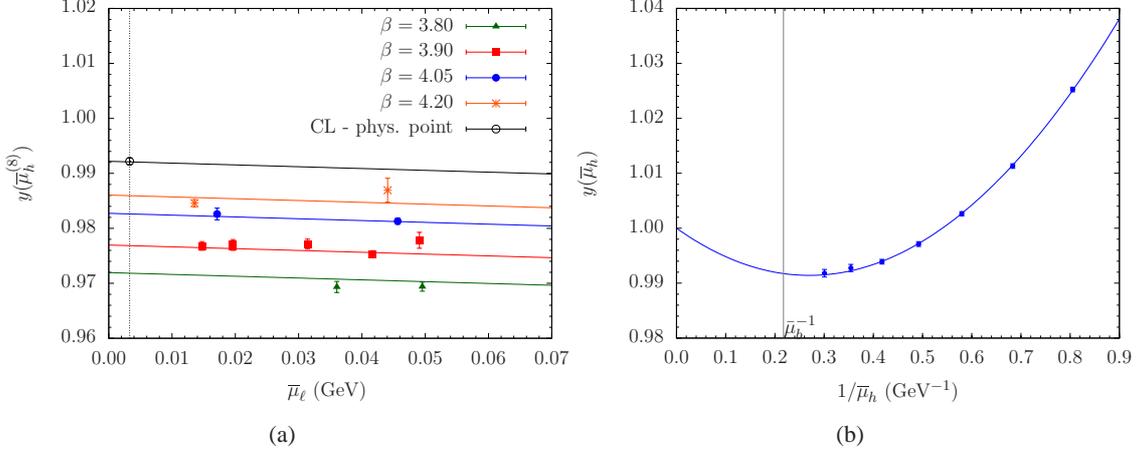

Figure 1: (a) Combined chiral and continuum fit of the ratio of heavy-light pseudoscalar meson mass for our largest value of the heavy quark mass (empty black circle is our estimate at the physical u/d quark mass in the continuum limit). (b) $y(\overline{\mu}_h)$ against $1/\overline{\mu}_h$ using the fit ansatz (3.3) ($\chi^2/d.o.f. = 0.3$).

follow analogous strategies to compute the heavy-strange pseudoscalar decay constant, f_{Bs}, and the value of the ratio of the heavy-strange and the heavy-light decay constants, f_{Bs}/f_B. We then get our estimate for the heavy-light pseudoscalar decay constant from $f_B = f_{Bs} / (f_{Bs}/f_B)$. Statistical errors are estimated using the bootstrap method. Our results read

$$f_{Bs} = 228(5)(6)[8] \text{ MeV}, \quad f_B = 189(4)(7)[8] \text{ MeV}, \quad f_{Bs}/f_B = 1.206(10)(22)[24]. \tag{3.6}$$

As a byproduct of our analysis we obtain the values of the pseudoscalar decay constants for the D_s and D mesons as well as for their ratio:

$$f_{Ds} = 250(5)(5)[7] \text{ MeV}, \quad f_D = 208(4)(6)[7] \text{ MeV}, \quad f_{Ds}/f_D = 1.201(7)(20)[21] \tag{3.7}$$

Error coding is as in Eq. (3.5).

4. Computation of bag parameters and ξ

The $\Delta B = 2$ effective weak Hamiltonian in its most general form reads

$$\mathscr{H}_{\text{eff}}^{\Delta B=2} = \frac{1}{4} \sum_{i=1}^{5} C_i \mathscr{O}_i + \frac{1}{4} \sum_{i=1}^{3} \tilde{C}_i \tilde{\mathscr{O}}_i, \tag{4.1}$$

with

$$\mathscr{O}_1 = [\overline{b}^\alpha \gamma_\mu (1-\gamma_5) q^\alpha][\overline{b}^\beta \gamma_\mu (1-\gamma_5) q^\beta], \quad \mathscr{O}_2 = [\overline{b}^\alpha (1-\gamma_5) q^\alpha][\overline{b}^\beta (1-\gamma_5) q^\beta],$$

$$\mathscr{O}_3 = [\overline{b}^\alpha (1-\gamma_5) q^\beta][\overline{b}^\beta (1-\gamma_5) q^\alpha], \quad \mathscr{O}_4 = [\overline{b}^\alpha (1-\gamma_5) q^\alpha][\overline{b}^\beta (1+\gamma_5) q^\beta],$$

$$\mathscr{O}_5 = [\overline{b}^\alpha (1-\gamma_5) q^\beta][\overline{b}^\beta (1+\gamma_5) q^\alpha], \quad \tilde{\mathscr{O}}_1 = [\overline{b}^\alpha \gamma_\mu (1+\gamma_5) q^\alpha][\overline{b}^\beta \gamma_\mu (1+\gamma_5) q^\beta]$$

$$\tilde{\mathscr{O}}_2 = [\overline{b}^\alpha (1+\gamma_5) q^\alpha][\overline{b}^\beta (1+\gamma_5) q^\beta], \quad \tilde{\mathscr{O}}_3 = [\overline{b}^\alpha (1+\gamma_5) q^\beta][\overline{b}^\beta (1+\gamma_5) q^\alpha]. \tag{4.2}$$

4

In Eqs (4.2) $q \equiv d$ or s, α and β denote color indices and spin indices are implicitly contracted within square brackets. The Wilson coefficients C_i and $\tilde{C}_i$ have an implicit renormalization scale dependence which is compensated by the scale dependence of the renormalization constants of the corresponding operators. The parity-even parts of the operators $\mathscr{O}_i$ and $\tilde{\mathscr{O}}_i$ are identical. Due to parity conservation in strong interactions it is sufficient to consider the matrix elements where only the parity-even components of the operators $\mathscr{O}_i$ enter. In the SM only the matrix element of the operator $\mathscr{O}_1$ enters. The bag parameters, B_i ($i = 1, \ldots, 5$), are defined through the equations

$$\langle \overline{B}_q^0 | O_1(\mu) | B_q^0 \rangle = \mathscr{C}_1 B_1^{(q)}(\mu) \, m_{B_q}^2 f_{B_q}^2 \tag{4.3}$$

$$\langle \overline{B}_q^0 | O_i(\mu) | B_q^0 \rangle = \mathscr{C}_i B_i^{(q)}(\mu) \left[\frac{m_{B_q}^2 f_{B_q}}{m_b(\mu) + m_q(\mu)} \right]^2 \quad \text{for } i = 2, \ldots, 5, \tag{4.4}$$

with $\mathscr{C}_i = (8/3, -5/3, 1/3, 2, 2/3)$. We have used a mixed fermionic action setup to evaluate the four-fermion matrix elements as it offers the advantage that matrix elements are at the same time O(a)-improved and free of wrong chirality mixing effects [11]. Four-fermion RCs have been computed using RI/MOM techniques in [12].

Since in the static limit each of the five bag parameters is a constant, we can apply the ratio method adopting a strategy analogous to the one used for the b-quark mass. For more details on the computation of ratios of bag parameters the reader is referred to Ref. [1]. In Table 1 we report our results in the $\overline{\text{MS}}$ scheme of Ref. [13] at the scale of the b-quark mass.

$(\overline{\text{MS}}, m_b)$				
$B_1^{(d)}$	$B_2^{(d)}$	$B_3^{(d)}$	$B_4^{(d)}$	$B_5^{(d)}$
0.85(3)(2)[4]	0.72(3)(1)[3]	0.88(12)(6)[13]	0.95(4)(3)[5]	1.47(8)(9)[12]
$B_1^{(s)}$	$B_2^{(s)}$	$B_3^{(s)}$	$B_4^{(s)}$	$B_5^{(s)}$
0.86(3)(1)[3]	0.73(3)(1)[3]	0.89(10)(7)[12]	0.93(4)(1)[4]	1.57(7)(8)[11]

Table 1: Continuum limit results for $B_i^{(d)}$ and $B_i^{(s)}$ ($i = 1, \ldots, 5$), renormalized in the $\overline{\text{MS}}$ scheme of Ref. [13] at the scale of the b-quark mass. Error coding is as in Eq. (3.5).

We also apply the ratio method to compute the SU(3)-breaking ratios $B_1^{(s)}/B_1^{(d)}$ and the important $\xi = (f_{B_s}/f_{B_d})(B_1^{(s)}/B_1^{(d)})^{1/2}$ parameter. In Fig. 2(a) and (b) we display the dependence on the inverse heavy quark mass of the appropriate ratios for $B_1^{(s)}/B_1^{(d)}$ and ξ, denoted as $\zeta_\omega(\overline{\mu}_h)$ and $\zeta_\xi(\overline{\mu}_h)$, respectively. For $B_1^{(s)}/B_1^{(d)}$ and ξ we obtain (see Ref. [1] for details)

$$B_1^{(s)}/B_1^{(d)} = 1.007(15)(14)[21], \quad \xi = 1.225(16)(26)[31]. \tag{4.5}$$

Our results for the quantities $f_{B_q} \sqrt{B_i^{(q)}}$ ($i = 1, \ldots, 5$ and $q = d/s$) can be found in Table 4 of Ref. [1].

5. Model-independent constraints on $\Delta B = 2$ operators and NP scale from UTA

The NP generalisation of the UT analysis is carried out by including matrix elements that, though absent in the SM, may appear in the theoretical parametrisation of various observables in
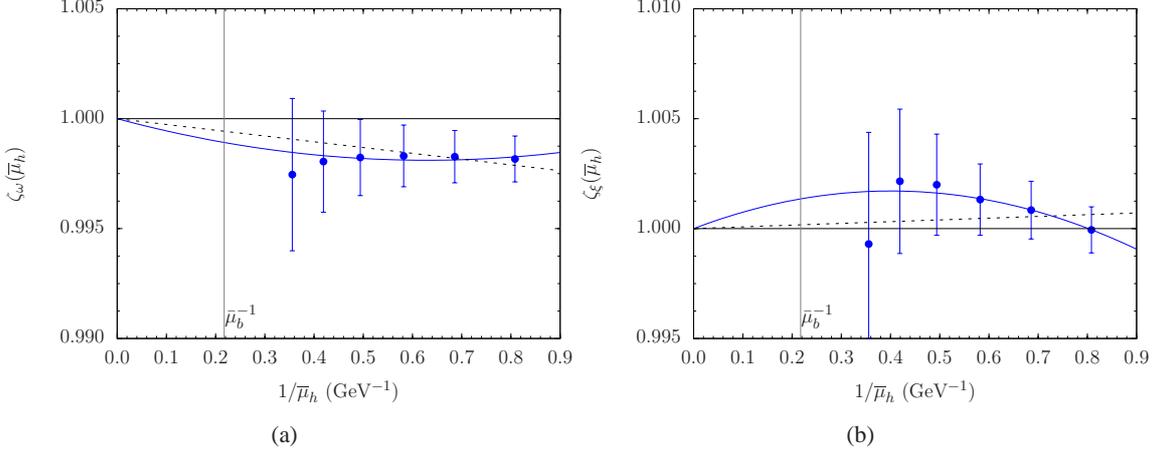
Figure 2: $\zeta_\omega(\overline{\mu}_h)$ and $\zeta_\xi(\overline{\mu}_h)$ against $1/\overline{\mu}_h$ are shown in panels (a) and (b), respectively. For both cases the fit function has a polynomial form of the type given by Eq. (3.3) (blue curve). In both panels a fit of the form $\zeta(\overline{\mu}_h) = 1 + \eta/\overline{\mu}_h$ is also performed (black dashed straight line). The vertical black thin line marks the position of $1/\overline{\mu}_b$.

extensions of the SM. We employ our unquenched lattice QCD results for the bag parameters of the full basis of the $\Delta B = 2$ four-fermion operators to update the UT analysis beyond the SM presented in Ref. [14]. The effective weak Hamiltonian, Eq. (4.1), is parameterized by Wilson coefficients of the form $C_i(\Lambda) = (F_i L_i)/(\Lambda^2)$ with $i = 2, \ldots, 5$. We denote by F_i the (generally complex) relevant NP flavor coupling, by L_i a (loop) factor which depends on the interactions that generate $C_i(\Lambda)$, and Λ is the scale of NP, i.e. the typical mass of new particles mediating $\Delta B = 2$ transitions. Hence, the phenomenologically allowed range for each of the Wilson coefficients can be translated into a lower bound on Λ. Other assumptions on the flavor structure of NP correspond to different choices of the F_i functions.

Following Ref. [14], we derive the lower bounds on the NP scale Λ by setting $L_i = 1$ which corresponds to strongly-interacting and/or tree-level coupled NP. Two other interesting possibilities are provided by loop-mediated NP contributions with L_i proportional to either α_s^2 or α_W^2. The first case corresponds for example to gluino exchange in the minimal supersymmetric SM, while the latter applies to all models with SM-like loop-mediated weak interactions. To obtain a lower bound on Λ entailed by loop-mediated contributions, one simply has to multiply the bounds we quote below by $\alpha_s(\Lambda) \sim 0.1$ or $\alpha_W \sim 0.03$, respectively.

Our analysis is performed (as in [14]) by switching on one coefficient at a time in each sector, thus excluding the possibility of having accidental cancellations among contributions of different operators. Thus in the case of accidental cancellations the bounds will be weaker.

In Tables 2 and 3 we collect the results for the upper bounds on the $|C_i^{B_d}|$ and $|C_i^{B_s}|$ coefficients and the corresponding lower bounds on the NP scale Λ. The superscript B_d or B_s is to remind that we are reporting the bounds coming from the B_d- and B_s-meson sectors we are here analyzing. In the present analysis both experimental and theoretical inputs have been updated with respect to Ref. [14] (see Ref. [15]). The constraints on the Wilson coefficients of non-standard operators and, consequently, on the NP scale turn out to be significantly more stringent than in Ref. [14], in

particular for the B_s sector. Comparing with the results of the UT–analysis in Ref [12], we notice that (at least for generic NP models with unconstrained flavour structure) the bounds on the NP scale coming from K^0–$\bar{K}^0$ matrix elements turn out to be the most stringent ones.

	95% upper limit (GeV^{-2})	Lower limit on Λ (TeV)
$|C_1^{B_d}|$	$4.7 \cdot 10^{-12}$	$4.6 \cdot 10^2$
$|C_2^{B_d}|$	$3.0 \cdot 10^{-13}$	$1.8 \cdot 10^3$
$|C_3^{B_d}|$	$1.1 \cdot 10^{-12}$	$9.5 \cdot 10^2$
$|C_4^{B_d}|$	$9.5 \cdot 10^{-14}$	$3.2 \cdot 10^3$
$|C_5^{B_d}|$	$2.7 \cdot 10^{-13}$	$1.9 \cdot 10^3$

Table 2: 95% upper bounds for the $|C_i^{B_d}|$ coefficients and the corresponding lower bounds on the NP scale, Λ, for a strongly interacting NP with generic flavor structure ($L_i = F_i = 1$).

	95% upper limit (GeV^{-2})	Lower limit on Λ (TeV)
$|C_1^{B_s}|$	$5.6 \cdot 10^{-11}$	$1.3 \cdot 10^2$
$|C_2^{B_s}|$	$4.9 \cdot 10^{-12}$	$4.5 \cdot 10^2$
$|C_3^{B_s}|$	$1.8 \cdot 10^{-11}$	$2.3 \cdot 10^2$
$|C_4^{B_s}|$	$1.6 \cdot 10^{-12}$	$7.9 \cdot 10^2$
$|C_5^{B_s}|$	$4.5 \cdot 10^{-12}$	$4.7 \cdot 10^2$

Table 3: 95% upper bounds for the $|C_i^{B_s}|$ coefficients and the corresponding lower bounds on the NP scale, Λ, for a strongly interacting NP with generic flavor structure ($L_i = F_i = 1$).

References

[1] N. Carrasco *et al.* arXiv: 1308.1851 [hep-lat].

[2] B. Blossier *et al. JHEP* **1004** (2010) 049, arXiv: 0909.3187 [hep-lat].

[3] P. Dimopoulos, *et al. JHEP* **1201** (2012) 046, arXiV: 1107.1441 [hep-lat].

[4] N. Carrasco *et al.* PoS(LATTICE2013)313.

[5] Ph. Boucaud *et al. Phys. Lett.* **B650** 304 (2007), arXiv: hep-lat/0701012.

[6] Ph. Boucaud *et al. Comput. Phys. Commun.* **179** (2008) 695, arXiv: 0803.0224.

[7] R. Baron *et al. JHEP* **1008** (2010) 097, arXiV: 0911.5061.

[8] R. Frezzotti and G.C. Rossi, *JHEP* **08** (2004) 007, arXiv: hep-lat/0306014.

[9] M. Constantinou *et al.*, *JHEP* **08** arXiv: 1004.1115.

[10] B. Blossier *et al.*, *Phys. Rev.* **D82** (2010) 114513, arXiv: 1010.3659.

[11] R. Frezzotti and G. C. Rossi, *JHEP* **10** (2004) 070, arXiv: hep-lat/0407002.

[12] V. Bertone *et al.*, *JHEP* **1303** (2013) 089, arXiv: 1207.1287.

[13] A. Buras, M. Misiak, and J. Urban, *Nucl. Phys.* **B586** (2000) 397–426, arXiv: hep-ph/0005183.

[14] **UTfit** , M. Bona *et al.*, *JHEP* **0803** (2008) 049, arXiv: 0707.0636.

[15] http://www.utfit.org/UTfit.